2000

Metal Dissolution Kinetics in Aluminum Etch Tunnels

Yongsug Tak
Iowa State University

Nishant Sinha
Iowa State University

Kurt R. Hebert
Iowa State University, krhebert@iastate.edu

Metal Dissolution Kinetics in Aluminum Etch Tunnels

Abstract
The potential dependence of the metal dissolution current density of aluminum in etch tunnels was measured, using pulsed increases of current during galvanostatic etching experiments. Etching was carried out in 1 N HCl solution at 65°C, and was followed by analysis of the topographic development of the dissolving surfaces using scanning electron microscopy. By manipulation of the current waveform, the dissolving area and the applied current were varied independently. Parallel experiments with current interruptions were used to help identify the area of the dissolving surfaces during the anodic pulse, which were shown to be submicron size patches on the tunnel tip surfaces. After correction for solution-phase potential drops, the current was found to obey an exponential Tafel dependence on potential. Measurements of the dissolved depth vs. time show that the rate of cathodic hydrogen evolution is significantly increased during the anodic pulse, by comparison with that at the more negative potentials during constant current etching. Good agreement of the present current-potential relation was obtained with that derived from the measurements of pit currents in thin films by Frankel *et al.* [*J. Electrochem. Soc.*, 143, 1834 (1996)].

Disciplines
Chemical Engineering

Comments
This article is from *Journal of the Electrochemical Society* 147 (2000): 4103–4110. Posted with permission.

Journal of The Electrochemical Society, **147** (11) 4103-4110 (2000)
S0013-4651(00)02-012-7 CCC: $7.00 © The Electrochemical Society, Inc.

Metal Dissolution Kinetics in Aluminum Etch Tunnels

Yongsug Tak,*,[a] Nishant Sinha,[b] and Kurt R. Hebert*,[z]

Department of Chemical Engineering, Iowa State University, Ames, Iowa 50011, USA

The potential dependence of the metal dissolution current density of aluminum in etch tunnels was measured, using pulsed increases of current during galvanostatic etching experiments. Etching was carried out in 1 N HCl solution at 65°C, and was followed by analysis of the topographic development of the dissolving surfaces using scanning electron microscopy. By manipulation of the current waveform, the dissolving area and the applied current were varied independently. Parallel experiments with current interruptions were used to help identify the area of the dissolving surfaces during the anodic pulse, which were shown to be submicron size patches on the tunnel tip surfaces. After correction for solution-phase potential drops, the current was found to obey an exponential Tafel dependence on potential. Measurements of the dissolved depth *vs*. time show that the rate of cathodic hydrogen evolution is significantly increased during the anodic pulse, by comparison with that at the more negative potentials during constant current etching. Good agreement of the present current-potential relation was obtained with that derived from the measurements of pit currents in thin films by Frankel *et al*. [*J. Electrochem. Soc*., **143**, 1834 (1996)].

Manuscript submitted February 3, 2000; revised manuscript received July 10, 2000.

The kinetics of the dissolution reaction in corrosion pits are of fundamental interest because they relate to the condition of the metal surface during corrosion and to the mechanism of metal dissolution. Metal dissolution in pits occurs at high current densities frequently exceeding 10 A/cm^2, and is often found to be controlled by ohmic resistance or mass transport, as opposed to surface kinetics. For pitting of aluminum in chloride solutions, the topic of this work, measurements of the potential dependence of the pit current density have been carried out by a number of investigators, who have focused on the growth of pits at potentials positive to the pitting and repassivation potentials.[1-7] Hunkeler and Böhni found that the pit current increases with potential and is controlled by the ohmic resistance of the pit solution.[2,3] Frankel and co-workers investigated the growth of two-dimensional pits in thin aluminum films and noted a potential region above the pitting potential in which the pit current increased with potential, and at higher potentials a current plateau which was ascribed to mass-transport limited dissolution.[1,4] Like Hunkeler and Böhni, they concluded that the first region was controlled by ohmic resistance. Beck's studies of artificial pits in concentrated $AlCl_3$ solutions also revealed ohmic-controlled dissolution with mass transport control at very high potentials (greater than 5 V *vs*. saturated calomel electrode).[5] On the other hand, Wong and Alkire[6] and Buzza and Alkire[7] generated single pits on aluminum using, respectively, localized ion implantation and laser irradiation, and found that the pit dissolution is controlled by mass transport at all potentials, consistent with the presence of an aluminum chloride salt film on the pit surface.

Without a clear picture of the kinetics of the dissolution reaction, it is difficult to predict the conditions necessary for ohmic or mass-transport control of the corrosion rate. The reason no prior study has found surface kinetic control of dissolution is partly related to the typical system parameters of pitting experiments, especially electrolyte conductivity and pit size. For example, the relatively dilute electrolyte solutions and large pits (order of 0.1 mm size) in the work of Hunkeler and Böhni would promote large pit ohmic resistances. If attention were directed at small pits and more conductive solutions were used, surface kinetic control might be observed. In fact, Strehblow and Wenners studied the growth of micrometer-size pits on iron and nickel, and found potential-dependent dissolution rates which were believed to be controlled by surface kinetics.[8,9]

The present work extends this principle to aluminum, focusing on dissolution of etch tunnels. Etch tunnels are pits produced by anodic etching in concentrated and highly conductive chloride ion-containing solutions at temperatures above 60°C.[10] They maintain approximately constant widths of about 1 μm as they penetrate the metal along <100> crystallographic directions to depths up to 100 μm. The corroding tip, or end surface of a tunnel is a (100) plane which dissolves at current densities of 6-25 A/cm^2, while the sidewalls are covered with an oxide film inhibiting dissolution. Tunnels originate from cubic etch pits, the predominant corrosion structures when the etching time is less than 1 s.[10] The electrode potential during tunnel growth is typically constant with time, and equivalent to the repassivation, or protection, potential of aluminum (E_R).[11,12] As in most metal/electrolyte systems, the E_R of aluminum decreases with increasing chloride concentration. Analysis of mass transport in tunnels reveals that as tunnels grow, the potential at the tip decreases and the chloride concentration there increases, such that the tip is continuously maintained very close to E_R.[11,12] While the tapered shape of long tunnels has been shown to be consistent with the presence of a nearly saturated $AlCl_3$ solution at the tip,[11,13] the present work concerns short tunnels (length of 10 μm) which have not begun to taper.

The metal dissolution rate in tunnels has been determined on time scales of seconds during constant current etching experiments,[10,14,15] as well as on time scales of milliseconds during transient experiments in which the current is stepped to lower values.[16] In the former experiments, the potential is equal to E_R, while in the latter ones it is more negative than E_R. Both types of measurement yield a constant dissolution rate of 2.1 μm/s (equivalent to a current density of 6.1 A/cm^2) for 1 N HCl etchant at 65°C, the conditions of this work. The tunnel dissolution rate depends on the temperature and composition of the etchant bath, but is independent of tunnel length.[10,14] In contrast to tunnel dissolution, the current density in etch pits can be as large as 20-30 A/cm^2 when they initially appear, but it then decays in a time of about 20 ms to the constant current density found in tunnels grown at the same etching conditions.[17,18] The large current density above E_R might be expected given the potential dependence found by Hunkeler and Böhni, and Frankel. Overall, these studies suggest that the tunnel current density is constant at or below E_R, and increases above this potential.

This work seeks to clarify the kinetic behavior of aluminum metal dissolution, through measurements of the dissolution rate in etch tunnels at potentials anodic to E_R. Anodic current pulses during galvanostatic etching experiments are used to stimulate the tip surfaces to corrode momentarily at current densities exceeding the constant steady-state values. The current-potential relation for the corroding surface is determined by analysis of the accompanying potential transients. The potential data are corrected for ohmic potential

* Electrochemical Society Active Member.
[a] Present address: Department of Chemical Engineering, Inha University, Inchon, Korea.
[b] Present address: Micron Technology, Boise, ID.
[z] E-mail: krhebert@iastate.edu

S0013-4651(00)02-012-7 CCC: $7.00 © The Electrochemical Society, Inc.

drops inside and outside tunnels as well as concentration overpotentials in tunnels, taking advantage of previous measurements of the cell ohmic resistance,[19] as well as model predictions of the internal concentration and potential fields inside tunnels.[12,20] The interpretation of the electrochemical measurements is aided by microscopic observations of the topographic changes on the tip surfaces caused by the anodic current pulses.

Experimental

Aluminum samples for etching are annealed 99.98% purity, 100 μm thick foils, which were manufactured for use as electrolytic capacitor electrodes. A high proportion of the surface grains have a (100) orientation, and the typical grain size is 100 μm. When the foils are etched for prolonged times, individual etch tunnels penetrate the entire foil without changing direction, indicating that grains span the foil thickness. Solutions were prepared from reagent grade chemicals.

The aluminum electrodes were prepared for etching by immersion in 1.0 N NaOH solution for 20 min at room temperature, followed by a wash with distilled water. This pretreatment enhances the number of tunnels formed during etching and the uniformity of their length distribution.[19] Etching was carried out under galvanostatic polarization, using a potentiostat/galvanostat (EG&G PAR 273), in 1 N HCl solution at a temperature of 65°C. During etching, aluminum samples were clamped into a glass holder which exposes 5.07 cm^2 of surface, and to which the platinum wire counter electrode was fixed. In this way, the ohmic resistance of the bulk etchant solution was held constant. The reference electrode (Ag/AgCl/4 M KCl, Fisher) was positioned behind the back plate of the holder and away from the current path between the working and counter electrodes. The measured potential was found to be insensitive to its exact location.

A personal computer was used to define the applied current waveforms, which were then transferred to the potentiostat with a GPIB-PC interface. Potential transients were measured and stored with a high speed voltmeter (Keithley 194A). For the current interruption and pulsed current reduction experiments, as in Fig. 1, the initial step reduction in current was applied at 5 s etching time. The morphology of the internal surfaces of etch tunnels was observed using scanning electron microscopy (SEM, JEOL JSM 840) with the help of an oxide replication technique.[21] Replicas of the etched surfaces were fabricated by first forming 80-90 nm thick anodic oxide films on the etched surfaces, and then dissolving the metal in a bromine/methanol solution. The anodic film left by this procedure serves as a replica of the etched metal surface. Heights of dissolution features within the tunnels were measured by comparing images taken at two stage tilt angles.

Results and Discussion

The purpose of the anodic current pulses is to stimulate increased metal dissolution in existing tunnels. However, to properly interpret the experiments, it is important to account for the effects of the anodic current pulses on other electrochemical processes as well, namely, the nucleation of new pits and oxidation on the filmed portion of the surface. For this purpose, two parallel sets of experiments were carried out, one in which the anodic pulses follow current interruptions, and the other where they follow pulsed current reductions. Figure 1 shows the general applied current waveform which describes both types of experiments, and defines the waveform parameters used in the later discussion. Values of these parameters are given in the figure captions for individual experiments. A period of 5 s at applied current density i_{a1} served to initiate tunnels and grow them to a length of about 10 μm. The anodic pulse is the period of duration t_H with applied current density i_{a3}. An intermediate period at lower current density i_{a2} immediately precedes the anodic pulse; in current interruption experiments, i_{a2} is zero, while in pulsed current reduction experiments, i_{a2} is between zero and i_{a1}.

During the current interruptions, the entire dissolving tunnel tip surfaces are covered with oxide film and thereby passivated. On the other hand, the current reductions from i_{a1} to i_{a2} cause only a fraction of the dissolving tip surface area to be covered with oxide, while the remainder continues to dissolve.[16,20] Thus, anodic pulses after current interruptions will include only phenomena specific to oxide-covered surfaces, such as nucleation of new pits, oxide film growth, and metal dissolution through the oxide layer. Anodic pulses after current reductions, in addition to these current sources, also include continuing dissolution from the portion of the tip surface which was not covered with oxide at the time of the current reduction. It is shown in the following that by comparing the two kinds of experiments, the potential dependence of this continuing dissolution current can be identified. The results of current interruption experiments are discussed in the next section, followed by those of pulsed current reduction experiments.

Morphology after current interruption experiments.—In experiments where the current was held constant for several seconds and then turned off, tunnel tip surfaces appear flat and featureless (Fig. 2a). The other micrographs in Fig. 2 show tunnel tip surfaces after experiments where anodic current pulses were applied after current interruptions. The anodic pulse time (t_H) in these experiments is 2 ms, and the interruption times (t_L) are 1, 8, and 40 ms. When t_L is 1 ms, the tip surfaces are fairly flat, but roughened by comparison with the case of no anodic current pulse. A large number of small pit-like features are found when t_L is 8 ms. However, when the interruptions are 40 ms or longer, the tip surface is again flat (Fig. 2d). The further development of tip surface morphology after current interruptions was investigated by increasing t_H to 20 ms (Fig. 3); here, i_{a3} is 10 mA/cm^2, and t_L is 4 ms in Fig. 3a, and 40 ms in Fig. 3b. As a result of continued metal dissolution during the longer anodic current pulse, distinct pits become apparent on the tip surfaces. These pits evidently grow from roughness features like those in Fig. 2c, suggesting that the surface roughness at t_H of 2 ms is due to localized dissolution at a very early stage. The number of pits is significantly smaller when the interruption time is 40 ms, as opposed to 4 ms. When the interruption is 40 ms or longer, pits still form near the tunnel tip during the anodic pulse, but are as likely to be found on the sidewalls near the tip as on the tip itself.

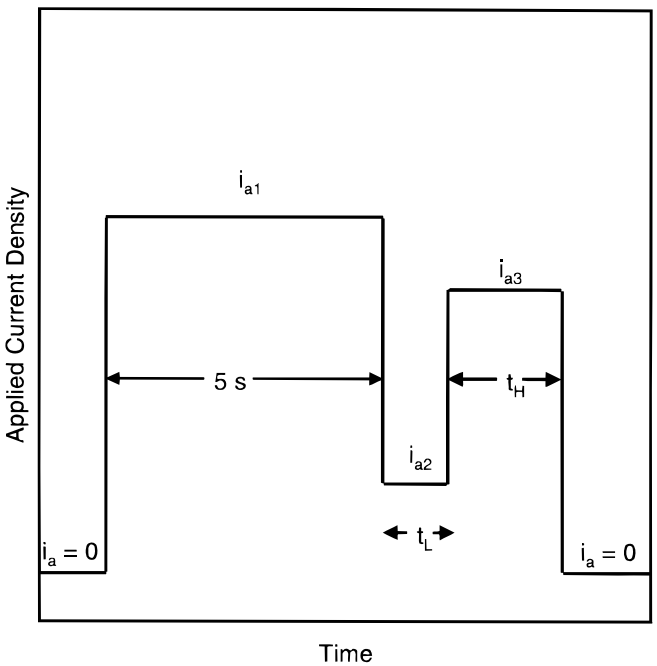

Figure 1. Schematic of applied current waveform, showing definitions of experimental variables. The anodic pulse is the period of length t_H when the applied current density is i_{a3}. i_{a2} is zero for the current interruption experiments, and between zero and i_{a1} for the pulsed current reduction experiments.

S0013-4651(00)02-012-7 CCC: $7.00 © The Electrochemical Society, Inc.

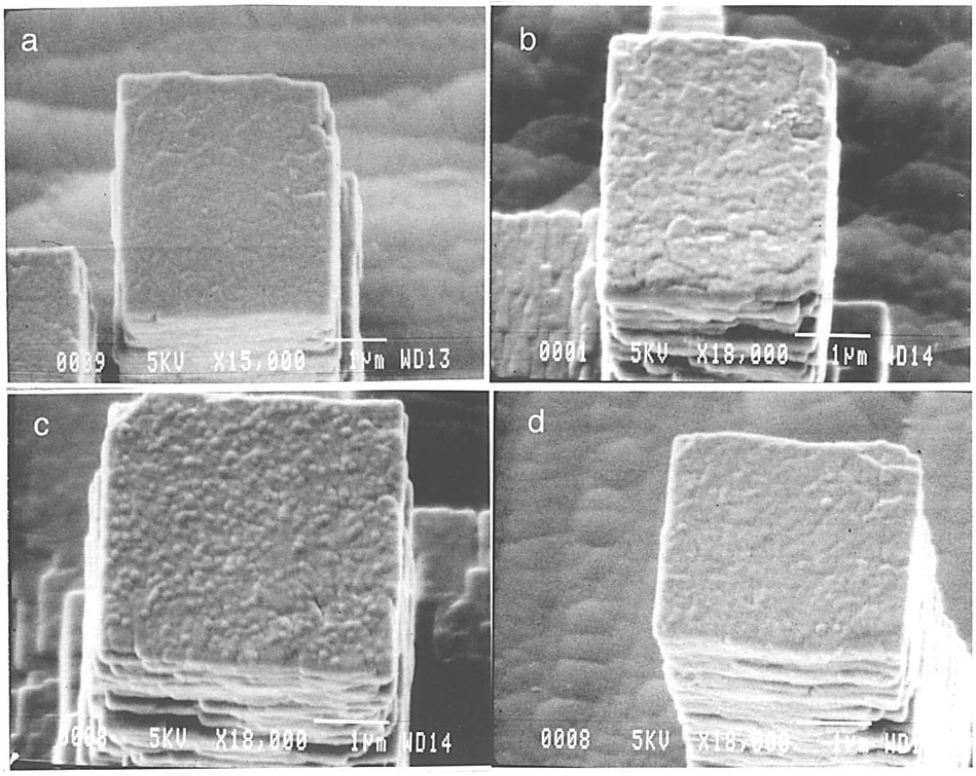

Figure 2. SEMs of replicas of tunnel tip surfaces after current interruption experiments, showing the effect of interruption time when the current pulse time t_H is 2 ms. (a) Current set to zero after 5 s at the applied current density (i_{a1}) of 40 mA/cm^2. For (b)-(d), t_H is 2 ms, i_{a2} is zero, and i_{a1} and i_{a3} are 40 mA/cm^2. (b) t_L is 1 ms; (c) t_L is 8 ms; (d) t_L is 40 ms.

Pit formation during anodic current pulses after very short interruptions of a few milliseconds implies that an oxide film is present on the tip surface at the time of the anodic pulse. This is expected, since Tak and Hebert showed that interruptions as short as 100 μs are sufficient to form an oxide layer on the tip surface.[20] The high incidence of pit formation on the tunnel tip, for t_L less than 40 ms, indicates that the newly formed oxide film there has a large number of pitting sites. The number of pit sites decreases with interruption time, such that nucleation no longer occurs exclusively on the tip when the interruption time is longer than about 40 ms. At longer interruption times, the continued preference for pit nucleation near, but not necessarily on, the tip can be explained by the presence of an enhanced chloride concentration in the solution near the tip. Hebert and Alkire found that the time for diffusion to effect changes in the solution composition inside tunnels is approximately 2 L^2/D, where L is the tunnel length and D is the diffusivity of the $AlCl_3$ electrolyte in the tunnel (about 2×10^{-5} cm^2/s for the present experimental conditions).[11] Since the present tunnels are 10 μm long, the diffusion time is about 100 ms, larger than the interruption times of 40 ms. Hence, the chloride concentration near the tip would still be significantly elevated compared to the bulk etchant solution, enhancing the likelihood of pit nucleation there when the anodic current pulse is applied.

Potential transients for current interruption experiments.—Figure 4 shows potential transients during anodic current pulses following interruptions. When the interruption time is 100 μs, the smallest in Fig. 4, the potential returns abruptly to the steady-state potential, with no significant overshoot. For the longer interruptions, there is an appreciable potential overshoot above the steady-state potential. The transient for the interruption time of 80 ms forms an envelope which all the other transients follow up to a point, before falling to the steady-state potential. This 80 ms transient consists of a rapid increase up to the potential E_a in the figure, after which the potential increases relatively more slowly to a maximum, and then falls to the steady-state potential. The times at which the other transients fall away from the 80 ms transient increase with increasing t_L.

The roles of the various current sources during the current pulse are elucidated by faradaic current-potential curves constructed from the potential transients. The faradaic current density (i_f) is obtained by subtracting the capacitive charging current density from the applied current density

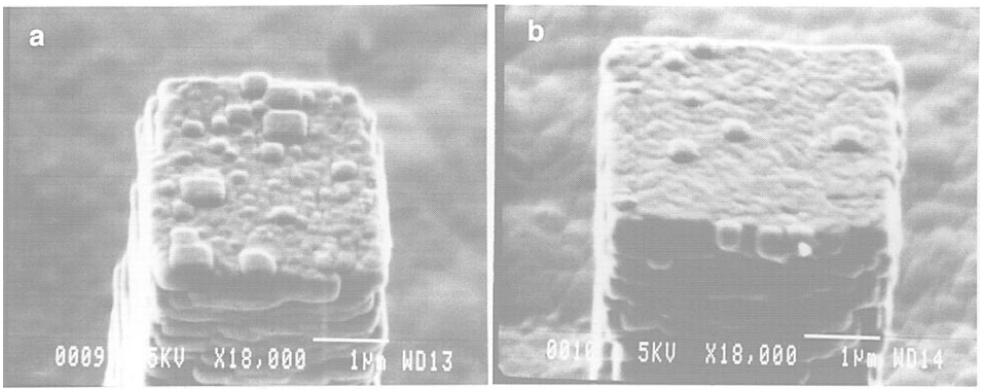

Figure 3. SEMs of replicas of tunnel tip surfaces after current interruption experiments, showing the effect of interruption time when the current pulse time t_H is 20 ms. i_{a2} is zero; i_{a1} and i_{a3} are 40 and 10 mA/cm^2, respectively. (a) t_L is 4 ms; (b) t_L is 40 ms.

S0013-4651(00)02-012-7 CCC: $7.00 © The Electrochemical Society, Inc.

$$i_f = i_a - C\frac{dE}{dt} \quad [1]$$

C, the capacitance, was calculated from the initial slopes of the potential transients and found to be 5.7 μF/cm^2, in agreement with the capacitance of 6.3 μF/cm^2 obtained from other experiments for the same etchant solution and temperature.[19] The resulting current-potential curves are shown in Fig. 5. The potential transients trace upward along these curves from the bottom. For t_L less than 40 ms, each curve can be divided into three regions: region 1, an increase of faradaic current with potential; region 2, an almost discontinuous jump of the faradaic current to a higher value; and region 3, a decrease of faradaic current with decreasing potential, until the applied current and the faradaic current are balanced. The current jump is at the peak potential of the transients in Fig. 4, and with larger interruption time, it occurs at a higher potential. The magnitude of the current jump for the experiments shown is nearly the same, 28 ± 1 mA/cm^2. From the potential transients, the elapsed time during the jump is no greater than 30 μs. The curves for t_L of 40 and 80 ms follow the same behavior as the others in region 1, but the jump does not occur. Instead, the faradaic current remains constant for a period of time at the applied current, while the potential increases at a constant rate up to its maximum. After the potential maximum, the faradaic current slowly increases and finally decreases back to the applied current.

The two shapes of current-potential curves in Fig. 5 (with and without current jumps) can be explained with reference to the SEM micrographs in the previous section. Current jumps are only present for the same experiments for which preferential pit nucleation on the tip surface occurs, that is, when the interruption is shorter than 40 ms. Thus, the current jumps (region 2) are associated with nucleation of pits on the tunnel tips. The current jumps may include both anodic dissolution and hydrogen evolution at pits. Since the time elapsed during the jumps is not more than 30 μs, this pit nucleation is very rapid. The short induction time and rapid nucleation are most likely due to the large number of pitting sites in the newly formed oxide film. Prior to the current jumps, the region 1 current in Fig. 5 is common to all the polarization curves, even those without jumps. This current is replotted in Fig. 6, using a logarithmic current axis,

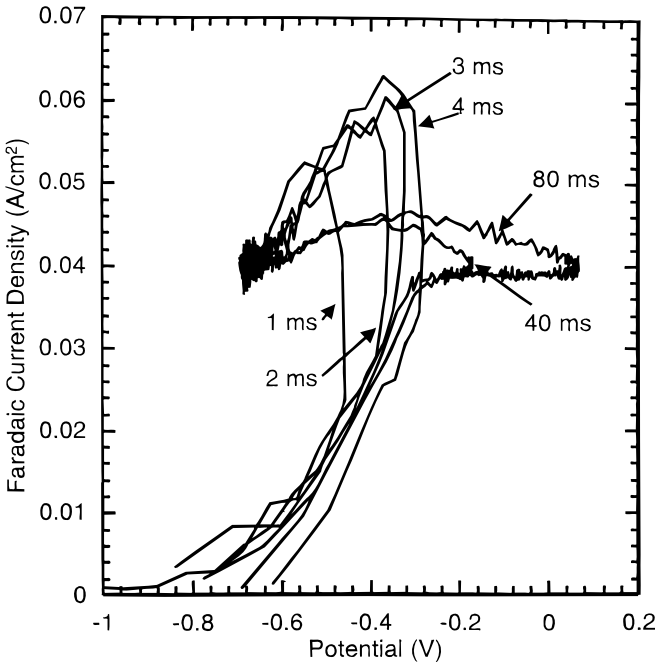

Figure 5. Variation of faradaic current with potential for the experiments in Fig. 4.

for the experiments with interruption times 4 ms or less. The current in region 3 is also shown after subtracting the current jump, thus removing the dissolution current from the newly formed pits on the tunnel tip. After the correction, the oxidation currents in regions 1 and 3 are roughly coincident, implying that the same electrochemical process determines the variation of current with potential in these two regions. They follow a Tafel-type kinetic expression of the form $i_{13} = i_{13}^0 \exp(b_{13}E)$, where i_{13}^0 and b_{13} are kinetic parameters. This kinetic expression is believed to represent metal dissolution through

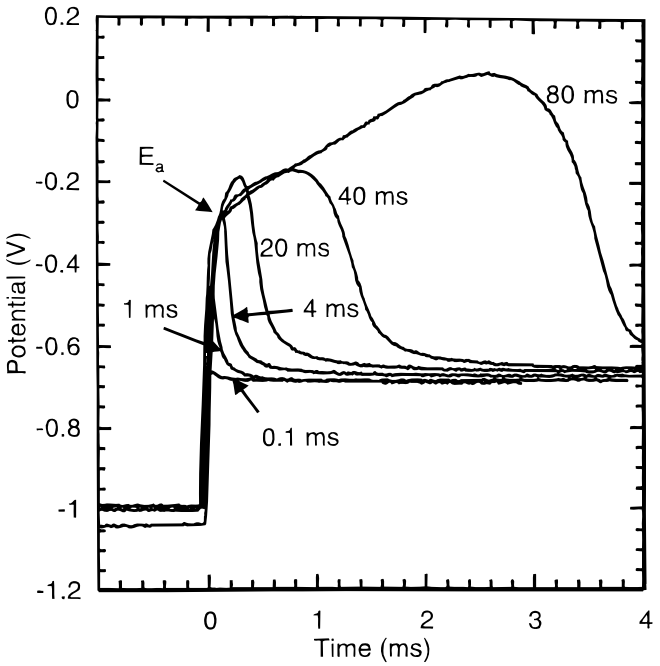

Figure 4. Potential transients during the anodic current pulse following current interruptions for variable interruption time t_L. i_{a2} is zero; i_{a1} and i_{a3} are both 40 mA/cm^2.

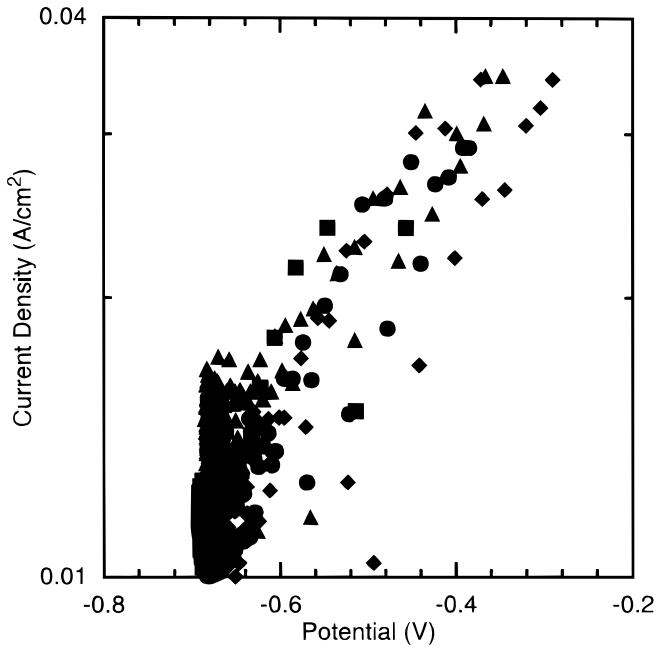

Figure 6. Variation of faradaic current with potential for the experiments in Fig. 4 with interruption times of 1, 2, 3, and 4 ms, in the region 1 and 3 portions of the faradaic current-potential plots (Fig. 5). The region 3 current was corrected before plotting by subtraction of the current jumps in Fig. 5. Interruption times are: (■) 1, (●) 2, (▲) 3, and (◆) 4 ms.

S0013-4651(00)02-012-7 CCC: $7.00 © The Electrochemical Society, Inc.

the oxide film on the tunnel walls and the external surface, since (*i*) no pits are present yet in region 1, and (*ii*) the Tafel form is consistent with measurements of the potential dependence of the dissolution rate of oxide-covered aluminum in acidic solutions.[22] A possible reason this current-potential relation is also followed in region 3 may be that the pitting current (including anodic dissolution and hydrogen evolution) is somewhat smaller than the oxidation current in this region, and perhaps less sensitive to potential.

The experiments without current jumps, *i.e.*, the 40 and 80 ms interruptions, are not plotted in Fig. 6, but also obey the Tafel expression up to E_a. After this point, the potential increases at a constant rate up to the potential maximum, while the faradaic current density remains constant, and no pit initiation occurs (Fig. 2 and 3). This behavior closely resembles potential transients during the initial growth of oxide films during galvanostatic oxidation in acidic solutions,[23] so that it probably also reflects film growth in the present experiments. Thus, E_a may be the potential at which the current in the film is sufficient for oxide growth to occur. The slow rise of the faradaic current above the plateau in Fig. 5 may be due to the nucleation of pits like those shown in Fig. 3b. This pit nucleation occurs over the time of the potential decays in Fig. 4 from the maxima, typically 1 ms. Thus, it is much slower than the rate of pit nucleation for interruption times 4 ms or smaller.

To summarize, the faradaic current during anodic pulses after current interruptions is supplied by a combination of pit nucleation and growth, and metal oxidation on the film-covered surface, the latter process resulting in either dissolution through the film or oxide growth. The potential transients in Fig. 4 identify the potential range for which these current sources are significant. Both the induction time prior to pit nucleation and the rate of pit nucleation are very strong functions of the age of the oxide film formed at the current interruption. For example, the induction time increases from about 0.1 to 3 ms as the age of the film increases from 1 to 80 ms. Since film growth may be significant during the interruption, an explanation for this result may be that the pit nucleation rate increases rapidly as the thickness of the oxide film decreases.

Morphology after pulsed current reduction experiments.—In the pulsed current reduction experiments, the applied current waveform follows Fig. 1, with i_{a2} greater than zero. Figure 7 shows a tunnel tip surface after an experiment in which i_{a2}/i_{a1} is 0.25, t_L is 12 ms and t_H is 4 ms. Well-defined raised "patches" are present, corresponding to areas where the rate of metal dissolution was larger than elsewhere. The patches resemble corrosion pits, but their morphology is distinct from that of the "pits" formed by anodic pulses after current interruptions. For experiments with comparable t_H and t_L (for example, see Fig. 7 and Fig. 2c), the patches are usually deeper than the pits, but the pits are more numerous. Pits may achieve similar depths as patches, but only after longer t_H (see Fig. 7 and 3a).

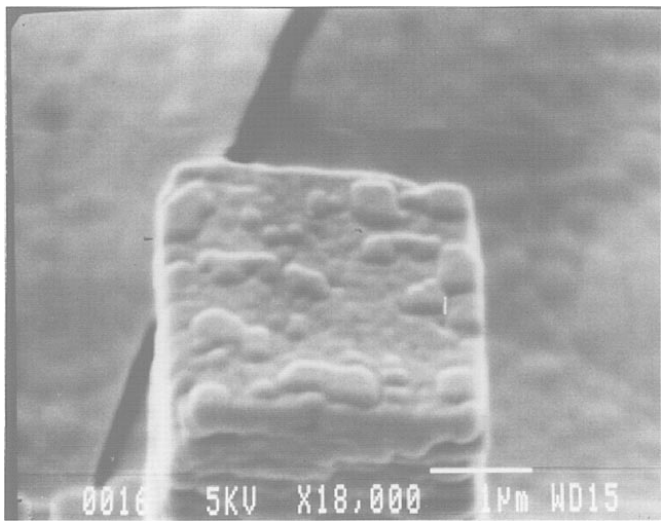

Figure 7. SEM of an oxide replicas of a tunnel tip surface following a pulsed current reduction experiment. t_H is 4 ms and t_L is 12 ms. i_{a1} and i_{a3} are 40 mA/cm^2, and i_{a2} is 10 mA/cm^2.

Patch structures like those in Fig. 7 were previously observed by Tak *et al*. after experiments where the current was stepped to a lower value i_{a2}, held there for periods (t_L) exceeding 5 ms, and then turned off (*i.e.*, $i_{a3} = 0$ in Fig. 1).[16] The patches in these prior experiments were identified as areas where the metal dissolution rate is the same (2 μm/s) as that prior to the current step to i_{a2}, while the surface surrounding the patches is passivated. Thus, oxide passivation at the time of the step leaves a fractional coverage of dissolving area equivalent to i_{a2}/i_{a1}. In the present experiments, the patches represent the same areas, but their dissolution rate is much larger than 2 μm/s. For example, the patches in Fig. 7 are about 0.1 μm high after only 16 ms growth time ($t_H + t_L$), giving a mean dissolution rate of about 60 μm/s, thirty times larger than in the experiments with no anodic pulse. Moreover, after experiments with the same t_L as in Fig. 7, but with no anodic pulse, the tip surfaces appeared flat in the SEM, and patch structures could be viewed only with atomic force microscopy (AFM).[16] Thus, the anodic current pulses in the present experiments stimulate a significantly enhanced metal dissolution rate on the patch areas formed by passivation at the time of the current step reduction.

Potential transients for pulsed current reduction experiments.—Figure 8 shows potential transients measured during the anodic current pulses following current reductions. The transients are for various values of i_{a2}, with i_{a3} set at 40 mA/cm^2 and t_L at 12 ms. These transients are characterized by a rapid rise to a maximum at about 50 μs, followed by a decay to an apparent plateau at about 1 ms. The maximum potentials are much more negative than those in Fig. 4 following current interruptions. Thus, the potential range in Fig. 4 is more negative than the potentials required to nucleate pits on the tip or wall surfaces in tunnels, or to provide significant dissolution current on the oxide-covered surface. In the absence of other current sources, it is concluded that the faradaic current during the anodic pulse is supplied from the active patches formed by the current re-

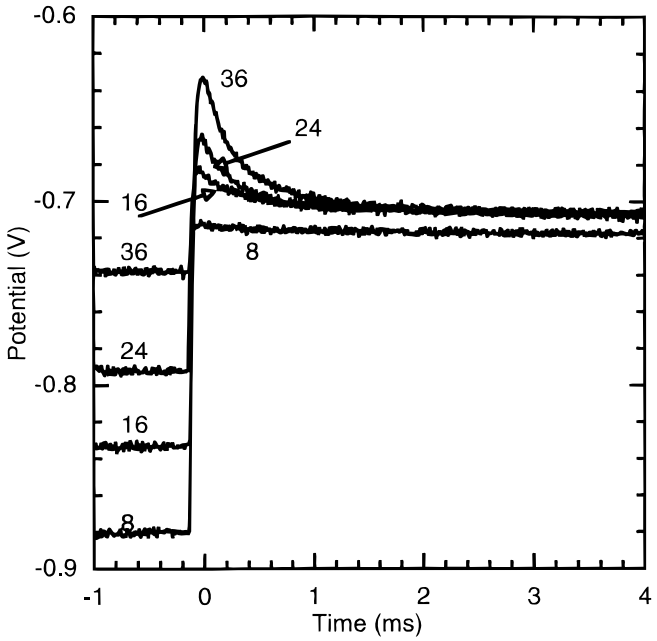

Figure 8. Potential transients during anodic current pulses following pulsed current reductions, showing the effect of i_{a2} (parameter in plot) at constant i_{a3} of 40 mA/cm^2. i_{a1} is 40 mA/cm^2 and t_L is 12 ms in all cases. Potentials of different transients are plotted without offset.

S0013-4651(00)02-012-7 CCC: $7.00 © The Electrochemical Society, Inc.

duction from i_{a1} to i_{a2}. In view of the potential rise during the anodic pulse, the large dissolution rate noted in Fig. 7 can be explained by potential-dependent dissolution kinetics.

The dependence of the patch current density on potential is determined using potential transients for experiments in which i_{a2} and i_{a3} are varied independently. Figure 9 shows i_{p2}, the patch current density just after the anodic current step, as a function of the corrected peak potential E_p, for a number of experiments with the same t_L of 12 ms. i_{p2} is $i_{p1}(i_{a3}/i_{a1})/(i_{a2}/i_{a1})$, where i_{p1} is the constant patch current density before the current step reduction and also during t_L. Since the hydrogen evolution current during constant current etching is only about 10% as large as the dissolution current density,[10] i_{p1} is well approximated by the tunnel dissolution current density, 6.1 A/cm^2 for these conditions. i_{a2}/i_{a1} represents the reduction of patch area compared to the entire tip, and i_{a3}/i_{a1} is the increase of total current during the anodic pulse. E_p is found by subtracting the ohmic potential drops both within tunnels and in the etching cell from the measured peak potential. The cell ohmic drop calculation uses the experimentally determined cell resistance of 2.17 Ω-cm^2 for the present etching conditions[19]; the calculation of the tunnel ohmic drop uses an effective conductivity of 0.1 (Ω-cm)$^{-1}$ for the tunnel solution, which was shown previously to yield good agreement with the detailed ohmic drop calculation.[20]

The data in Fig. 9 are from two sets of experiments: (1) varying i_{a2} from 8 to 36 mA/cm^2 while i_{a3} remains at 40 mA/cm^2, and (2) varying i_{a3} from 15 to 75 mA/cm^2 while i_{a2} is held at 10 mA/cm^2. In experiment set (1) the patch area during t_H is varied, while the total patch current is fixed, while in set (2) the patch area is constant, and the current during the anodic pulse is varied. Since the data for sets (1) and (2) appear to follow the same trend, the dependence of the patch current density on the potential is the same for both the current and area variations. Thus, the active electrode area is identified correctly as the patch area. The common behavior of the two data sets is also evidence for the accuracy of the ohmic correction, since the ohmic drop of set (1) is constant while that of set (2) is proportional to the current density. At current densities lower than 30 A/cm^2, the patch current density follows an exponential Tafel-type expression

$$i_p = i_{po} \exp(b_p E_t) \qquad [2]$$

where the kinetic parameters b_p and i_{po} are 16.0 V^{-1} and 7.11 × 10^6 A/cm^2, respectively, and E_t is the ohmic-corrected potential *vs.* the experimental reference electrode.

An additional Tafel plot (not shown) was constructed using the potential corrected for both ohmic and concentration overpotential. The concentration overpotential was calculated to be 62 mV for all the experiments, using the method of Zhou and Hebert and assuming steady-state diffusion.[12] This assumption is valid because the t_L of 12 ms is much smaller than the time constant for diffusion in tunnels of this length.[11] With this additional concentration overpotential correction, the resulting potential is equivalent to the repassivation overpotential defined by Zhou (*i.e.*, the difference between the potential and repassivation potential), augmented with an additive constant. Since the dissolution mechanism is not known beforehand, it cannot be used to guide the choice of whether the potential or the repassivation overpotential is the proper driving force. With the additional potential correction, the quality of the fit to the Tafel line is similar to that in Fig. 9, indicating that it is not possible to distinguish the two driving forces on an empirical basis either. The values of b_p and i_{po} obtained with both corrections are 19.2 V^{-1} and 2.83 × 10^7 A/cm^2, respectively.

As mentioned above, both dissolution and hydrogen evolution may be included in the patch current density in Eq. 2 and Fig. 9. The contribution of metal dissolution was determined by measurement of the increase of patch depth with time during the anodic pulse. Figure 10 shows average patch depths, for experiments with t_L set at 12 ms, i_{a1} and i_{a3} at 40 mA/cm^2, and i_{a2}/i_{a1} at 0.25. The patch depth at a t_H of zero corresponds to the expected dissolution during t_L, or 2.1 μm/s × 12 ms = 0.025 μm. The thick and thin lines in the figure represent two calculations of patch depth. The thin line was determined by applying the kinetic expression in Eq. 2 to the potential transient in this experiment. The patch depth h as a function of time was found by integration according to Faraday's law

$$\frac{dh}{dt} = \frac{\epsilon i_p(E_t)}{3FC_M} \qquad [3]$$

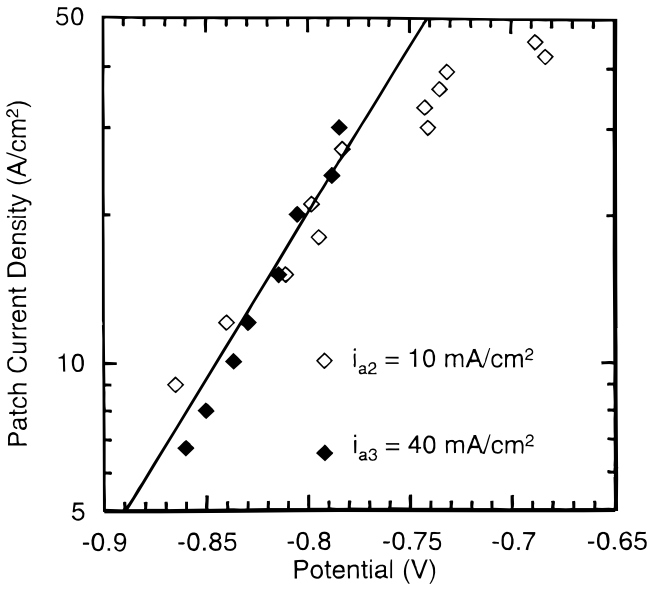

Figure 9. Relationship between patch current density at maximum potential of transients and maximum potential corrected for ohmic resistance. t_L is 12 ms in all cases. Solid symbols are from experiments with i_{a3} set to 40 mA/cm^2, and varying i_{a2}; open symbols represent experiments with constant i_{a2} of 10 mA/cm^2, and varying i_{a3}. Solid line is a regression fit to the data, excepting the six points with greatest current densities.

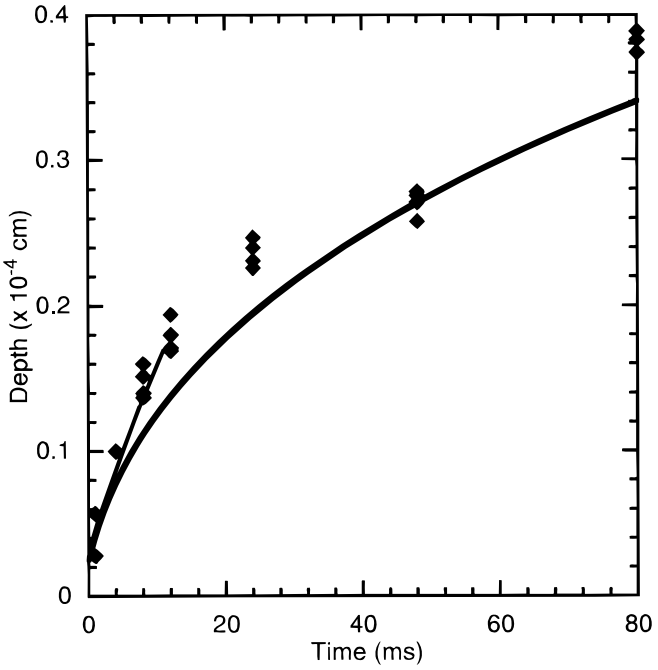

Figure 10. Influence of metal dissolution on the heights of corroding patches, as a function of the anodic pulse time t_H, with t_L set at 12 ms. i_{a2} was 10 mA/cm^2; i_{a1} and i_{a3} were both 40 mA/cm^2. Symbols are experimental data, thick line is calculation based on current balance, thin line calculation based on potential transient.

S0013-4651(00)02-012-7 CCC: $7.00 © The Electrochemical Society, Inc.

where ϵ is the current efficiency for metal dissolution and C_M is the concentration of aluminum atoms in the metal. ϵ was chosen as 2.2 in Fig. 10 to obtain agreement of calculated and measured patch depths. This value is much larger than the current efficiency of 1.1-1.2 typically measured during tunnel growth at constant current, and suggests an increased rate of hydrogen evolution during the anodic pulse.

The thick line in Fig. 10 represents a calculation based on a current balance on the dissolving patches, using the fitted current efficiency. In this calculation, it is recognized that as the patch depths increase, they develop actively dissolving sidewalls, and therefore expand in both width and depth.[24] Thus, the increasing active area requires that the patch current density decrease with time in order to maintain the constant applied current. The dissolution rate was taken to be uniform on the entire patch surface. i_t, the (constant) current per tunnel tip area, is then

$$i_t = ni_p[4(r_o + h)^2 + 8h(r_0 + h)] \qquad [4]$$

where n is the number of patches per tunnel tip area, and the initial patch width is $2r_0$. In Eq. 4, the patches are approximated as being uniform in size and square in cross section, and merging of adjacent growing patches is neglected. Equation 4 was substituted into Eq. 3 for $i_p(t)$, and the resulting differential equation was numerically integrated to obtain the patch depth h as a function of time. n was found from SEM micrographs to be 2.7×10^8 cm^{-2}, and r_0 was then determined as 0.26 μm from the current balance during t_L. The resulting calculated curve in Fig. 10 shows good agreement with the patch depth data, providing additional support for the validity of the current efficiency and the kinetic expression in Eq. 2.

The potential dependence of the electrochemical reactions studied in this work reveals unexpected and complex behavior. The current efficiency of 2.2 suggests that the cathodic hydrogen evolution current is 54% as large as the metal dissolution current during the anodic pulses. The large hydrogen evolution rate is thermodynamically possible since the potential is appreciably more negative than the rest potential of that reaction. However, it is surprising since during constant current etching the hydrogen current is only about 10% of the metal dissolution current[10]; one might have expected the rate of this cathodic reaction to decrease at the higher potentials found during the anodic current pulse. Additionally, the potential independence of the dissolution current density found below the steady-state etching potential contrasts with the strongly potential-dependent dissolution rate above it (Fig. 9). Taken together, these observations suggest that the potential dependences of these electrode processes are complex and would be unexpected from simple kinetic laws such as the Butler-Volmer equation. It is likely that the reaction rates are influenced not only by the potential itself, but also by the potential-dependent nature of films or adsorbed layers on the dissolving surface. Possibly, these layers are appreciably different above and below the steady-state etching potential. The steady-state potential has been identified as the repassivation potential of aluminum.[12] The different behavior of both metal dissolution and hydrogen evolution with respect to this potential suggests differences in surface layer composition above and below it.

The dissolution kinetic measurements reported here can be compared to those of Frankel *et al.*, who investigated the potential dependence of the current density of two-dimensional pits in aluminum thin films in NaCl solutions at room temperature.[1,4] They measured the dissolution and total current densities of the pit with use of microscopic observation of the evolution of pit geometry. The dissolution current density was found to increase with potential and decrease with film thickness, with the data for various films following separate trends when plotted *vs.* potential. Since the inverse slope of the current-potential curve for the experiment in 0.1 M NaCl was within 20% of the calculated ohmic resistance,[4] it was concluded that dissolution is controlled by ohmic resistance, in agreement with Hunkeler and Böhni,[2,3] but unlike the surface kinetic control exhibited in the present measurements. However, the data in 1 M NaCl (Fig. 1 in Ref. 1) might be under mixed ohmic-surface kinetic control because of the higher conductivity of this solution. Hence, these latter data were corrected for ohmic resistance to determine whether the resulting current-potential relation agrees with the present kinetic results.

In Fig. 11, the dissolution currents from Ref. 1 are plotted against the potential corrected for the pit ohmic resistance. The ohmic correction follows Pierini and Newman's formula for the primary resistance of a ring electrode[4,25]

$$\Delta\phi_\Omega = \frac{ix}{\kappa}\left\{0.2313\pi - \frac{1}{2\pi}\ln\left[1 - \left(\frac{r_1 - x}{r_1}\right)^3\right]\right\} \qquad [5]$$

where $\Delta\phi_\Omega$ is the ohmic potential drop, i the dissolution current density, κ the conductivity, x the film thickness, and r_1 the pit radius. κ was taken as 0.1 $(\Omega\text{-cm})^{-1}$ and r_1 as 0.032 cm. While the actual radius is not known, the results were found to be insensitive to r_1 as it was varied between 0.005 to 0.1 cm. This is expected since when the thickness-radius ratio of a ring is small, its resistance is nearly the same as that of a strip electrode.[25] With this ohmic correction, the data for the four thickest films collapse into a single trend very similar to that in Fig. 9, *i.e.*, an exponential Tafel-type kinetic expression with a deviation to lower currents at current densities above about 30 A/cm^2. This deviation may be due to the approach to a mass-transport limited, potential-independent condition, as found by Frankel.[4] In the Tafel region, the current density obeys $i_d = i_{d0}\exp(b_d E)$, where b_d is 25.3 V^{-1} and i_{d0} is 5.08×10^9 A/cm^2; the slope b_d is similar to that from the present work, as illustrated by the dashed line in Fig. 11. This line represents the Tafel expression using the ohmic and concentration potential corrected potential. The different magnitude of the preexponential current density may be explained partly by the temperature difference between the experiments in Fig. 9 and 11, and partly by the small potential offset between the standard calomel electrode (SCE) reference electrode in Ref. 1 and the Ag/AgCl/4 N KCl electrode in the present work (about 40 mV at room temperature).

In any case, it is clear from Fig. 11 that there is a strong consistency between these very different kinetic measurements, which val-

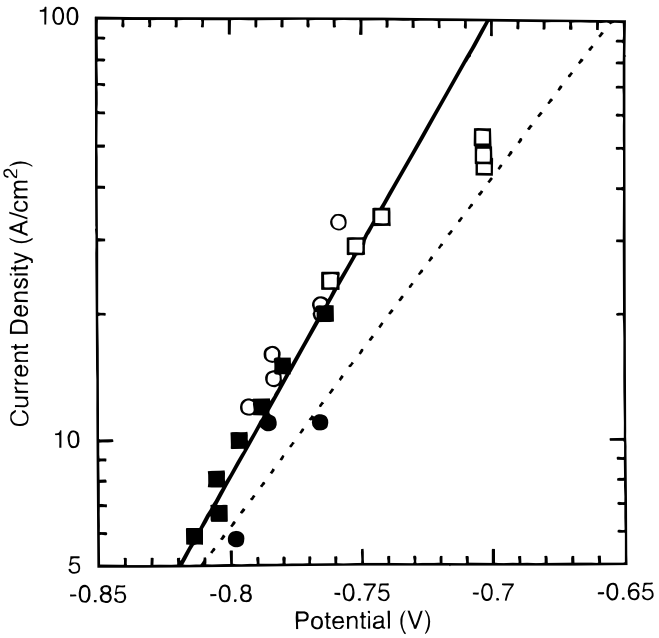

Figure 11. Relationship between dissolution current density and potential in 1 M NaCl at room temperature from aluminum thin film experiments of Frankel *et al.*[1] Potential is with respect to SCE, and is corrected for ohmic resistance. Symbols are experimental current densities for films with thicknesses of 330 Å (open squares), 1430 Å (open circles), 4250 Å (closed squares), and 9670 Å (closed circles). Solid line is a regression fit to the data, excepting those with the three highest current densities, and the dashed line is the fit line from Fig. 9, with no reference electrode correction applied.

S0013-4651(00)02-012-7 CCC: $7.00 © The Electrochemical Society, Inc.

idates both sets of results. The pit currents of Frankel *et al.*[1] are influenced primarily by surface kinetics, and not ohmic resistance, because of the relatively small surface area to volume ratio of the thin film pits, along with the conductive 1 M NaCl solutions used in their work. It also should be noted that the time scale of the present dissolution measurements are significantly smaller than those of the thin-film experiments. For example, Frankel's current measurements are averaged over tens of seconds, compared to the time of only 0.1 ms for the transient potential response in Fig. 8. The agreement of the two sets of measurements, despite the different experimental time scales, suggests that the dissolution rate is uniform in time, at least over the potential range where Tafel behavior is observed. Thus, dissolution does not proceed by intermittent bursts.

The knowledge gained in the present work can be applied to previous observations about pit growth at early times. Dissolution current densities as large as 100 A/cm^2 were measured here at anodic potentials, typical of the range of values interpreted from pit growth rates from millisecond time scale etching experiments.[17] Hence, the transient burst of dissolution sometimes found when a pit first nucleates may be the result of an initially high dissolution rate consistent with Eq. 2. This pit current density would then decrease rapidly as the pit grows and its ohmic drop builds up, causing the potential at the dissolving surface falls to more negative values, and eventually approach as a limiting value the constant value found close to the repassivation potential. This behavior was in fact observed by Lin and Hebert.[18]

Conclusions

Anodic current pulses were applied during anodic galvanostatic tunnel etching of aluminum, to investigate the kinetics of the metal dissolution reaction. The pulses, typically a few milliseconds in duration, were applied after a reduction of applied current for a period of a several milliseconds. When the reduced current prior to the anodic pulse is set to zero (current interruption experiments), the dissolving tunnel tip surface is passivated at the time of the interruption. The anodic pulse then produces nucleation of new pits on the tip and wall surfaces of tunnels, as well as dissolution and oxide growth on the passive surface. The induction time for pit nucleation is only 0.1 ms for a 1 ms interruption time, and increases strongly as the interruption time is increased. Hence, the newly formed oxide on the tip surface contains a large density of pitting sites, but the number of these sites decreases strongly as the film is allowed to develop and perhaps grow in thickness during the interruption.

In experiments with the reduced current larger than zero, the current reduction causes the tip surface to partially passivate, leaving patches of dissolving surface surrounded by oxide film. During the subsequent anodic current pulses, the applied current is supplied primarily by enhanced metal dissolution from these patches. The kinetic relation between the dissolution current density and the potential (corrected for solution phase potential drops) was investigated through experiments in which both the dissolution area and the applied current during the pulse were varied independently. All these experiments produce a consistent dependence of patch current density on potential, which follows a Tafel equation for current densities up to 30 A/cm^2, and deviates below this relation at higher current densities. Analysis of potential transients and patch depth measurements indicate that the rate of hydrogen evolution (the presumed cathodic process) is about five times larger during the anodic pulse compared to constant current etching. The current-potential relation is very similar to that derived from the thin film pitting experiments of Frankel *et al.*,[1] after those results were corrected for ohmic resistance. This agreement is despite the much smaller time scale of the present kinetic measurements, indicating that dissolution proceeds uniformly in time. The present measurements along with Frankel's are believed to be the first which reveal the surface kinetics of aluminum dissolution in pits, a process which is normally under ohmic or mass-transport control.

Acknowledgment

This work was partially supported by KDK Corporation (Takahagi, Japan), who also provided the aluminum foils used for etching.

References

1. G. S. Frankel, J. R. Scully, and C. V. Jahnes, *J. Electrochem. Soc.*, **143**, 1834 (1996).
2. F. Hunkeler and H. Böhni, *Corrosion*, **37**, 645 (1981).
3. F. Hunkeler and H. Böhni, in *Proceedings of the International Congress on Metallic Corrosion*, Vol. 2, p. 163, National Research Council of Canada, Ottawa (1984).
4. G. S. Frankel, *Corros. Sci.*, **30**, 1203 (1990).
5. T. R. Beck, *Electrochim. Acta*, **29**, 485 (1984).
6. K. P. Wong and R. C. Alkire, *J. Electrochem. Soc.*, **137**, 3010 (1990).
7. D. W. Buzza and R. C. Alkire, *J. Electrochem. Soc.*, **142**, 1104 (1995).
8. H.-H. Strehblow and J. Wenners, *Z. Phys. Chem. N. F.*, **98**, 199 (1975).
9. K. J. Vetter and H.-H. Strehblow, in *Localized Corrosion*, NACE-3, p. 240, B. F. Brown, J. Kruger, and R. W. Staehle, Editors, NACE, Houston, TX (1974).
10. R. S. Alwitt, H. Uchi, T. R. Beck, and R. C. Alkire, *J. Electrochem. Soc.*, **131**, 13 (1984).
11. K. R. Hebert and R. C. Alkire, *J. Electrochem. Soc.*, **135**, 2146 (1988).
12. Y. Zhou and K. R. Hebert, *J. Electrochem. Soc.*, **145**, 3100 (1998).
13. D. Goad, *J. Electrochem. Soc.*, **144**, 1965 (1997).
14. K. R. Hebert and R. C. Alkire, *J. Electrochem. Soc.*, **135**, 2447 (1988).
15. E. Makino, T. Yajima, T. Shibata, M. Ikeda, Y. Tanno, and E. Suganuma, *Mater. Trans., JIM*, **34**, 796 (1993).
16. Y. Tak, E. Henderson, and K. R. Hebert, *J. Electrochem. Soc.*, **141**, 1446 (1994).
17. B. J. Wiersma and K. R. Hebert, *J. Electrochem. Soc.*, **138**, 48 (1991).
18. C.-F. Lin and K. R. Hebert, *J. Electrochem. Soc.*, **137**, 3723 (1990).
19. B. J. Wiersma, Y. Tak, and K. R. Hebert, *J. Electrochem. Soc.*, **138**, 371 (1991).
20. Y. Tak and K. R. Hebert, *J. Electrochem. Soc.*, **141**, 1453 (1994).
21. C. G. Dunn and R. B. Bolon, *J. Electrochem. Soc.*, **116**, 1050 (1969).
22. A. Despic and V. P. Parkhutik, in *Modern Aspects of Electrochemistry*, Vol. 20, p. 432, J. O'M. Bockris, R. E. White, and B. E. Conway, Editors, Plenum, New York (1989).
23. G. E. Thompson and G. C. Wood, in *Treatise on Materials Science and Technology*, Vol. 23, J. C. Scully, Editor, p. 253, Academic Press, New York (1983).
24. Y. Tak, Ph. D. Thesis, Iowa State University, Ames, IA (1993).
25. P. Pierini and J. Newman, *J. Electrochem. Soc.*, **125**, 79 (1978).